Exploring the chemical plane of Mg, Mn and Al in the search for extra-galactic stars in the Milky Way

Eleni Moschovaki

Division of Astrophysics
Department of Physics

LUND
UNIVERSITY

2024–EXA223

Degree project of 15 higher education credits
May 2024

Supervisors: Govind Nandakumar & Nils Ryde

Division of Astrophysics
Department of Physics
Box 118
SE-221 00 Lund
Sweden

Abstract

In this study, over 2000 Milky Way stars were analyzed in the [Mg/Mn] vs [Al/Fe] chemical plane to identify accreted stars. The Milky Way's faster star formation enriches disk stars with iron-peak elements such as Mn and reduces α elements like Mg. Accreted stars, originating from slower star formation rate environments, exhibit lower metallicities, reflected in lower [Al/Fe]. The study evaluates if non local thermodynamic equilibrium (NLTE) modeling, in contrast to local thermodynamic equilibrium (LTE), affects this distinction. Abundances were derived from APOGEE survey data (DR17) for 1944 disk stars and 88 potential accreted stars identified by Feuillet et al. (2022). Spectral synthesis under both LTE and NLTE was performed for 2032 stars, ensuring precise data collection. Diagnostic plots comparing LTE and NLTE abundance determinations revealed discrepancies. While LTE plots showed distinct patterns consistent with theoretical expectations, NLTE plots presented less clear distinctions. NLTE accreted stars exhibited lower [Al/Fe] but not consistently higher [Mg/Mn], indicating NLTE's significant impact on abundance determinations. These findings underscore the importance of NLTE considerations and show that for NLTE calculations, the diagnostic graph is no longer useful.

Populärvetenskaplig beskrivning

Vår galax, Vintergatan, är en något större än normalt, stavspiralgalax. Som en sådan stor galax har den förmågan att rymma enorma massor av interstellärt medium (ISM), inklusive gas som utkastas från stjärnor när de exploderar till supernovor i slutet av sina liv. I denna explosion kastas tyngre element som producerats i stjärnan genom fusion ut. När denna process fortsätter och ISM fylls mer och mer med dessa tunga element, bildas nya stjärnor med en relativt större mängd av dessa grundämnen än tidigare stjärnor. Med tanke på att stjärnbildningshastigheten (SFR) är ganska hög i Vintergatan förutsäger teoretiska modeller att nyare stjärnpopulationer som är belägna i galaxens skiva är rika på dessa tunga element. Därför, om några stjärnor upptäcks i det området och deras halter av dessa tunga element är lägre än det som förutsägs, blir de kandidater för att vara extragalaktiska stjärnor.

Genom tidigare studier har vi sett att Vintergatan har sammansmällt av andra mindre galaxer i sitt förflutna och har "ätit upp" eller assimilerat dem. Detta har naturligtvis en inverkan på utvecklingen, formen hos vår galax. Anledningen till att kunskapen om vad som hände och kunna identifiera stjärnor som inte bildats på plats är viktig för att förutsäga och skapa bättre teoretiska och tillämpbara modeller om galaxers utveckling i allmänhet. Vi fokuserar på vår galax eftersom det är den vi bor i och därmed kan få mer detaljerade och tillförlitliga stjärnspektra. Spektra definieras som intensiteten av ljus som utsänds från en ljuskälla och har ett stort omfång som sträcker sig från infrarött och optiskt till ultraviolett. Infraröda spektra består av långa våglängder, vilket motsvarar lägre energier. Detta är fördelaktigt när ljus passerar genom många gasmoln som innehåller olika partiklar, och som känt interagerar ljus med materia men ju längre våglängd desto mindre interaktion eller spridning. Av den anledningen kommer högupplösta infraröda spektra att användas i detta arbete, erhållna av APOGEE projektet i deras DR17-dataversion. Spektrum från denna undersökning syntetiseras med hjälp av ett datorprogram.

Många studier hittills har gjort liknande tillvägagångssätt, men de har antagit lokalt termodynamisk jämvikt (LTE) av enkelhetsskäl. Denna modell antar att stjärnan strålar som en svart kropp och ignorerar alla andra externa strålningsfenomen. För detta arbete kommer en annan modell att implementeras, kallad icke-lokalt termodynamisk jämvikt (NLTE), som tar hänsyn till andra källor till strålning och försöker korrigera LTE-modellen. Med detta sagt kommer de tunga element som undersöks att vara magnesium (från SNII), aluminium (från SNII) och mangan (från SNIa). Med hjälp av dessa abundanser i både LTE och NLTE kommer dataplanet med axlarna [Mg/Mn] kontra [Al/Fe] att konstrueras för ett generellt urval av skivstjärnor och ett specifikt urval med antagna extragalaktiska stjärnor. Denna plot ska visa hur NLTE påverkar denna diagnostiska plot och syftar till att belysa vikten av att implementera ett sådant tillvägagångssätt för framtida studier och dra relevanta slutsatser.

Contents

Chapter 1

Introduction

A field of study concerned by many is the formation of our galaxy. The Milky Way is a later type galaxy which is said to be formed by mergers of smaller and bigger size galaxies which resulted to what it looks like now, a spiral barred galaxy (Renaud et al. (2021)). The reason we want to find out how our galaxy is formed is in order to understand how the forces of nature act macroscopically and expand our knowledge about the overall evolution of the universe. The reason why we use the Milky Way in that search is because we live in this galaxy and so information retrieved from it are more reliable. Therefore, finding stellar systems that are accreted in the Milky Way is a way of identifying and tracing past mergers and the reason why we use stars is being explained below.

Stellar spectroscopy serves an important purpose in astrophysics and in particular in the field of Galactic archaeology. Galactic archaeology is the study of the history of our Galaxy through observations of the different objects in it, especially stars. In this area, stars can be assumed to be the fossils of our galaxy which can reveal a significant amount of information about its past.

Retrieving this information is possible through stellar spectroscopy, the study of spectra obtained from the stars. In general, analysing spectra can give information about properties of the star, such as temperature, velocity, composition and the surface gravity.

The sky survey "Apache Point Observatory Galactic Evolution Experiment" (APOGEE) using two telescopes, one in the United States and one in Chile, was able to observe both the northern and southern skies and collect the spectra of around $675,000$ stars. The observations were done in near infra-red which is suitable for when one wants to study the inner parts of the Galaxy because near infra-red light can pass through different stellar gas/medium and also interstellar dust easier meaning without interacting with matter as much through scattering and thus getting less obscured. APOGEE has also provided its own corrections to the spectrum that needed to be made in order to tackle broadening effects due to our atmosphere for example, as well as micro- and macroturbulence, along with their own determined data for abundances.

The topic of this thesis is to determine abundances for Magnesium (Mg), Aluminum (Al) and Manganese (Mn) for both Local Thermodynamic Equilibrium (LTE) and non-LTE (NLTE) using line and continuum masks from Fridén (2023). The reason those elements are chosen is attributed to the fact that [Mg/Mn] vs [Al/Fe] plot acts as a diagnostics tool in the quest to pin down extra-galactic stars in our Galaxy (see Chapter 2.5). Yet, other studies such as,Vasini et al. (2023) and Feuillet et al. (2022), suggest that kinematic data is also need to be used along the abundances as an independent variable for identifying accreted stars. To determine and produce that data I will be examining around 2000 stars referred to as the APOKASC sample and comparing them with another sample of 88 accreted stars extracted from APOGEE using specific conditions that are suggested in Feuillet et al. (2022). Finally, the outcome of this project will be to determine whether the NLTE corrections play a role in the diagnostic plot and whether the abundances on their own with NLTE can be used solely to pick out those accreted stars in the Milky Way.

In the theoretical background chapter, I will mention and explain relevant terminology as well as concepts needed to understand this project. In the methodology, I will explain further how the data was gained and in the results that will be presented.

Chapter 2

Theoretical background

2.1 Infra-red spectroscopy

The data retrieved in this thesis come from spectroscopic measurements made in infra-red wavelengths (1000nm-5000nm). When trying to observe stellar objects, the telescopes receive the light illuminated from those objects and this light travels through the interstellar medium (ISM). The ISM is composed of gas clouds of different thicknesses and dust particles of various sizes could interact with the light/energy from and affect the final observed spectrum of a star (Gray (2022)). Therefore, the more energetic or bluer the light, the higher the probability of this light getting scattered and thus obscured in the medium. For that reason, longer wavelengths or redder light which is also known as infra-red is a more reliable source when observing distant luminous objects. Furthermore, this range of wavelengths, $1500\text{ nm} - 1700\text{ nm}$, is especially good when observing stars in the Milky Way and specifically in the Milky Way mid plane and towards the center. In those regions, the dust and extreme stellar crowding prevent observations in optical wavelengths ($360\text{ nm} - 830\text{ nm}$). This makes infrared wavelength ranges and infrared spectra in studying such dust obscured regions.

In more detail, it is good to mention the origin of light from stars and how the infra-red light that we collect from the stars is actually made. Nuclear fusion processes taking place inside the star which is the process by which lighter elements are fused with a tremendous amount of energy to create heavier elements. This gives the stars the ability to heat up and shine. The light produced originates from the core and it radiates in all directions, travelling through the gas that makes up the star. As this happens, the light rays are interacting with the gas molecules and atoms causing various excitations. The initial light rays are of a short wavelength because they are very energetic so they have a very high chance interacting with the medium and get scattered, thus the radiation we receive is actually due to the de-excitation of the atoms that got excited in the beginning (Gray (2022)). This gives then a range of different wavelengths in infra-red as well, that we can detect.

2.2 Broadening effects

Spectral lines can undergo broadening which can be the result of many different effects. Broadening in an elemental line changes the shape of it and there are three types of profiles attributed to this new shape; the Gaussian, the Lorentzian and the Voigt. The Voigt is described by the Hjerting function which is the mathematical description of the convolution between a Gaussian and Lorentzian profile (Gray (2022), Rutten (2003)). Having said that, each broadening effect has its own profile and in the case where there are more than two effects taking place in the same line, if the profiles are both Gaussian or Lorentzian the resulting one is Gaussian or Lorentzian respectively, otherwise a mix of them becomes a Voigt. As one can see from figure 2.1, the Voigt profile has the wings of a Lorentzian profile but the bell curve of a Gaussian profile.

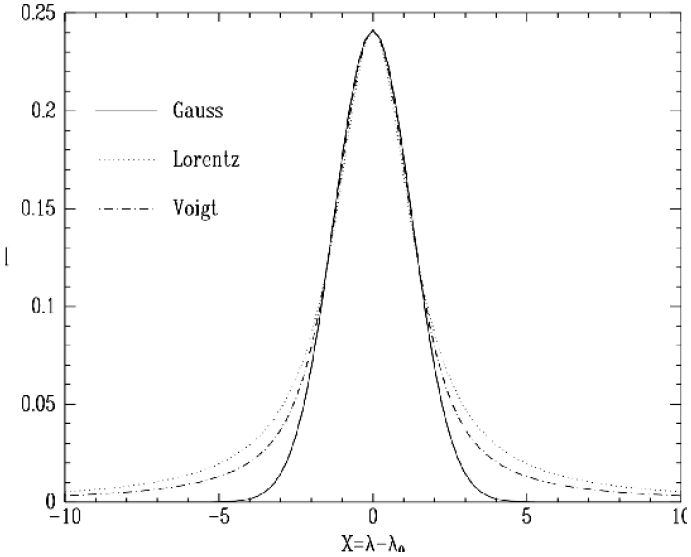

Figure 2.1: This figure shows the different profiles, the Gaussian with a black line, the Lorentzian with the dotted line and the Voigt with the dotted and normal line (Rocco & Cruzado (2012))

Now that we know the different mathematical shapes, we can go ahead and describe the different effects. Firstly, we have thermal (Doppler) effect which is due to thermal motion of gas which has a Gaussian profile and appears sharper for heavier elements (Gray (2022)). Secondly, natural broadening is a case related to the transition probability for spontaneous excitation from upper levels to lower levels per particle in the lower level, or in other words the Einstein coefficient. The damping constant of this effect is inversely proportional to the life time of the transition. It is extremely small, usually not resolved and has a Lorentzian profile. Another Lorentzian profile broadening process is collisional broadening. That includes effects such as pressure, Stark and Van der Waals forces in the medium. Lastly, we can also have non-thermal Doppler broadening effects that are

Gaussian such as micro- and macro- turbulence. Micro turbulence is of a scale less than a photon mean free path and it is created from random motion of small scale gas, causing turbulence inside it which affects line formation (Rutten (2003)). Macroturbulence is at a scale very much larger than the photon mean free path. The broadening is due to small gas 'blobs' in the medium moving relative to us in different directions, away or to us, causing them to be red or blueshifted (Gray (2022)). It is like a different source of a Doppler effect. Lastly, an effect less talked about is the hyperfine broadening. Hyperfine energies are usually calculated using first order perturbation theory, assuming that the energy splitting in the fine structure is relatively bigger (Andersson et al. (2015)). Yet, if we have a higher atomic mass number, it consists of more fine and hyperfine splitting levels and as a result some of the hyperfine splitting from different parents fine splits are interacting with each other. That is referred to in literature as off-diagonal interaction (Andersson et al. (2015)). This blending can lead to a broadening effect.

For this project, a bigger focus is around macroturbulence. Although theoretically macroturbulence is defined in the way described above, in this work encompasses other broadening factors which are the instrumental profile and the resolution of the spectrum. This macroturbulence in this project is referred to as "vmac" and even though it does not influence the strength of the lines, a good estimation of it is required to achieve better a fitting of a synthetic spectrum (Fridén (2023)). It is calculated using a set of six Fe I lines discussed more in section 3.2.

2.3 Abundances

As described in 2.1, there are a lot of nuclear processes taking place inside a star, with a lot of the light produced interacting with the constituents of gas cloud itself. In Earth, we have estimated theoretically and experimentally the different transition energies of almost all the elements, including hyperfine structure transitions. Hence, we can use this data to identify the lines in star spectrum corresponding to different elements. Longer wavelengths originate from transitions between energy levels that are closer and hence require less energy for the transition between the energy levels. The majority of a star is composed of hydrogen, therefore, astronomers have chosen hydrogen as reference point. The ratio between the number density cm^{-3} of the element X, in all states including ionization and molecular, and hydrogen H is taken as such (Gray (2022)):

$$A_X = \frac{N_X}{N_H} \tag{2.1}$$

However, that fraction results to a very low value since the most abundant component of a star is Hydrogen and so instead we take the logarithmic value of equation 2.1. Additionally, the most common way is to also express the abundances normalized with the solar values which is done by subtracting the ratios as such:

$$[X/H] = log_{10}(\frac{N_X}{N_H})_{star} - log_{10}(\frac{N_X}{N_H})_{sun} \tag{2.2}$$

The unit is called "dex" and the bracket notation characterises that normalization (Forsberg (2023)). In most cases, the abundance with respect to iron (Fe) is taken because there are many iron lines that one can determine accurately the abundance of and it can also act as an agent for time. Hence, the value of [Fe/H] is referred to as metallicity.

In any way, we can set the wavelength range to be including the transition wavelength of the element of interest when collecting the flux of a star. The strength of the absorption lines found in the respective wavelength in the total spectrum reflect the abundance of the element in the star. One can measure this quantity through calculating the depth or the strength of the line in different ways, for example, by modelling and fitting the observed spectrum with a synthetic spectrum and estimating the half width full maximum value. Yet, in order to do that it is important to know what stellar parameters can actually influence the strength of those lines in order to also model an accurate and precise synthetic spectrum.

A widely used method for approximating the depth of a line is called the "weak line approximation". This approach is estimating the area of the absorption line by calculating the same amount of area of a rectangle where the flux is 1 (Gray (2022)). The two areas must be the same and the equation used to derive this is the following:

$$W_\lambda = \int_{line} \frac{F_c - F_\nu}{F_c} d\nu \tag{2.3}$$

Solving this reduces to:

$$\begin{aligned} W &= \frac{\text{constant}}{\kappa_\nu} * \int_0^\infty l_\nu d\nu \\ W &= \text{constant} * \frac{\pi e^2}{m_e c} \frac{\lambda}{c} f \frac{N}{\kappa_\nu} \end{aligned} \tag{2.4}$$

depending on the wavelength, λ, the number of line absorbers per unit volume, N, the mass of electron, m_e, the oscillator strength, f, the speed of light, c, the electron charge, e, the continuous opacity constant κ_ν and the mathematical constant π. Once again, for values such as abundance and frequencies which can be very small, the logarithmic scale is used resulting in the final weak line approximation equation:

$$log(\frac{W}{\lambda}) = C + log(A) + log(gf\lambda) - \theta_{ex}\chi - log(\kappa_\nu) \tag{2.5}$$

As seen form equation 2.5, the final expression depends on the "gf"-value, the relative abundance of the species A, the inverse temperature,θ_{ex} [1], the excitation potential,χ and

[1]The inverse temperature is defined as $\theta_{ex} = 5040/T$

the continuous opacity absorption constant κ_ν. "f" represents the oscillator strength, or the probability of transition between specific energy levels in an atom and "g" is the statistical weight of the initial atomic level. W is divided by λ in order to normalize it to the wavelength to tackle its Doppler broadening. All these parameters are very crucial on defining the shape of the absorption line and it is good to know how each one can affect it.

If a star has a lot of hydrogen in a small area then the electron pressure grows and as a result we have more continuous bound-free processes taking place. Bound-free transitions are the source of the light we observe since it comes from the recombination light of H_{bf} (hydrogen) ion, meaning when a hydrogen atom captures a free electron from the previous ioinzation of H where the electron went from a bound state to a free one (Gray (2022)). Therefore, the continuous absorption coefficient is proportional to the electron pressure and according to equation 2.4, a higher opacity constant will decrease the equivalent width of the line. The implication of this when observing stars is that lines will be deeper in giants than in dwarfs. Thus, observing giants and specifically cooler giants is useful because we can determine elemental abundances reliably (Nandakumar et al. (2024)). The temperature also has a role in this due to Boltzmann's statistics.

Another stellar parameter that is not so straight forward from the above equations is the gravitational acceleration on the surface of a star, $log(g)$, which also has an impact on the observed lines. This value is defined as:

$$g = \frac{GM}{R^2} \tag{2.6}$$

with M the mass of the star, R the radius of it and G the gravitational constant. This value is of importance because for example if it is high, it indicates a more condensed star, thus making the pressure in the atmosphere higher and creating broader lines ($P_e \propto log(g)$). Moreover, it is dependent on temperature and has a less distinct effect which makes it hard to calculate through observations. Additionally, $log(g)$ values estimations also suffer from inaccuracies when spectroscopically deriving the radius of the star resulting in a non realistic value. Many methods have been developed for determining this value, three of which are: a)Ionization balance, b)Wings of strong lines and c)Astroseismology. The ionization method is simply deriving the abundances of an element from different lines in ground and ionized states, as at the end those values should be the equal, any difference in those values indicates the surface gravity. This is due to the surface gravity constant having an impact on the ionization of the elements. A common element used to derive the $log(g)$ value is iron and especially the Fe I and Fe II lines since they are more sensitive to the pressure of the star's atmosphere. However, there are some drawbacks with this method, for example not enough ionized Fe lines being available, not enough ionized lines that can be used for this process or in contrary, in the case of a hot star where usually we have non-thermodynamic equilibrium and over-ionization of Fe lines (Jofré et al. (2019)).

For method b), the uncertainties deriving the log(g) value from wings of strong lines

make this method not so reliable. In order to do this determination, elemental abundances must already be known and then the log(g) is calculated from the wings in strong lines created due to the pressure of the star. Because the pressure broadening parameters must be accurately known as well, which is challenging, this method is not as trustworthy. Moreover, the wings are not very much affected by log(g), rather the pressure affects them more which then makes it hard to determine accurate values. The uncertainties are around 0.2 dex which is deemed too high to be used (Jofré et al. (2019)). Lastly c), astroseismology is one of the more accurate methods. As the name suggests, log(g) and even other stellar parameters such as effective temperature or mass are determined by observing and analysing the stellar pulsations. The same way seismic waves gives information about Earth's composition, similar waves released by a star can give similar information about log(g). The uncertainties using this process are as low as 0.01 dex (Jofré et al. (2019)).

2.4 LTE and NLTE

When modeling stellar atmospheres, we assume that the atmosphere, or the plasma in a stellar atmosphere, to be represented as an one-dimensional hydrostatic model and the spectrum is formed under local thermodynamic equilibrium (LTE). NLTE and LTE are models that are only used when fitting absorption lines and not in the whole spectrum. Since the modeling is initially done in LTE for the whole spectrum we are observing, in order to apply NLTE in the lines we want to determine the strength of, we need to calculate the departure coefficient which shows how far off the LTE assumptions are from the NLTE. This is described in more detail later in the text.

In LTE it is implied that external or internal radiation that change the population level of the ground state of ions through collisions, is not taken into account. Therefore, the line strength which depends in the population levels, is determined through Saha-Boltzman statistics and the Maxwelian velocity distribution(Bergemann & Nordlander (2014)). As a result, the radiation field equals the Planck function, $J_\nu = B_\nu$.

On the other hand, the other model, NLTE is assuming that scattering also plays an important role. Deep inside the star, where the mean free path of the photon is less than the change in temperature and change in pressure, we can assume local dynamics (energy emission). However, in the outer layers the mean free path becomes larger, the Plank function diverges from the Source function resulting in an anisotropic, non-local radiation field. The Saha-Boltzman statistics are replaced by statistical equilibrium which is describing when the change of an energy level through time is zero (Bergemann & Nordlander (2014)).

$$\frac{dn_i(r)}{dt} = \sum_{i \neq j}^{N} n_j(r) P_{ij}(r) - n_j(r) \sum_{i \neq j}^{N} P_{ij}(r) = 0 \tag{2.7}$$

where $P_{ij} = C_{ij} + R_{ij}$, denotes the total collisional and radiative rates per particle and j denotes the bound or free energy state in a bound-bound or bound-free transition, whereas i the ground one. As a result we have a coupled system of the statistical equilibrium and radiative transfer equations which must be solved simultaneously to retrieve the distribution of particles in the excited levels. The solution is not trivial and a lot of computational power is needed, yet the effect that NLTE has on the ion lines is important. In order to understand and estimate how far the LTE model is from the NLTE model, we need to investigate the departure coefficient (Bergemann & Nordlander (2014):

$$b_i = \frac{n_{NLTE}}{n_{LTE}} \tag{2.8}$$

n_{NLTE} and n_{LTE} denotes the number density of a given energy level in an atom or a molecule calculated for each of the two cases. If $b_i = 1$ then we have LTE, but if $b_i < 1$ then NLTE is underpopulated and similarly, $b_i > 1$, NLTE is overpopulated (Bergemann & Nordlander (2014)). For the $b_i < 1$ case, it shows that the line opacity is being decreased and the line formation depth increases, therefore, the temperature gets higher deeper in the star impacting the line formation by weakening the absorption lines. On the contrary, when $b_i > 1$, the other way around holds, the line formation occurs in the outer layers of the star, temperature also lower in the outer layers thus strengthening of the absorption lines. Consequently, we see that the NLTE effects grow with increasing temperature. In more detail, the NLTE atomic processes that are typically taken into account when making such simulations, are divided into two categories: the photo-ionisation dominated atoms and the collision-dominated ions. In the former case, $b_i < 1$ which means there is a strong under-population of levels due to over-excitation and ionization of species and especially neutral atoms. This happens when the mean intensity exceeds the Plank function towards UV , $J_\nu > B_\nu$. Atoms that are greatly affected by this event are: Mg I, Al I, Si I, Ca I, Mn I, Fe I and Co I (Bergemann & Nordlander (2014)). Moreover, two stellar parameters that alter with the increase in NLTE effects are the decrease of the metallicity [Fe/H] and the decrease of the log(g) value. The latter atomic process mentioned, collision-dominated ions, occurs as an over-recombination event and/or as photon suction. Over-recombination is when the opposite of photo-ionization takes place.

2.5 Importance of Mg, Al and Mn

In the search for accreted stars, scientists have developed many ideas and different ways one can possibly identify such objects, yet it is still hard to tell which method is correct or not. Starting from N-body simulations of early merging events in the Milky Way, implying using only dynamical data, has been proven to not be enough (Ceccarelli et al. (2024)). The main reason for that is, the integral of motion simulations have shown formation of clumps and over-densities due to possible overlapping with data from different mergers. This results to plausible contaminated samples giving off wrong kinematic data and mistaking

the over-densities for independent Halo substructures. Therefore, in order to complement the kinematic data, scientists combined some independent parameters such as elemental abundances (Ceccarelli et al. (2024)). This method appears to be beneficial as it is known stars born into different chemical environments are also composed of different chemical abundances and have different star formation rates (SFR). Heavier elements, such as Mn, are products of type Ia supernovae (SNIa) whilst Al and Mg are said to be produced by supernova core collapses type II (SNII) (Matteucci (2021)). The difference between the two types is that type Ia supernovae originate from a binary star system where one of the stars has collapsed to a white dwarf, whereas the type II is through the core collapse of giant stars with more than 8 solar mass, which results in a major explosion (Das et al. (2020)), and therefore enriches the ISM on a shorter timescale.

In more detail, α-elements such as Mg, are mainly produced in short lived massive stars and expelled in the ISM through SNII. Al is not an iron-peak element or an α-element, instead it is formed through fusion in late stages of a star's life. It is also another element that is found in ISM though type SNII explosions. What is important for those kind of supernovae is that they produce relatively low Fe in comparison with the SNIa ones (Matteucci (2021)). The formation of Al is different for low and high mass stars. For high mass stars, it is produced during hydrostatic helium burning whilst for low mass stars it can be a product during the asymptotic giant branch state (AGB) Nandakumar et al. (2024). AGB is a phase that a cooler star of mass less than 8 solar mass will undergo where its interior is characterized by three main reactions. In the inner core of the star we have carbon and oxygen, in the shell surrounding the core we have fusion of helium atoms to carbon and in the shell after that we have the fusion of hydrogen to helium nucleii. During the early evolution of such stars, the main source of energy is helium fusion to carbon and the star swells up to giant star sizes. This is also referred to as the CNO (carbon-nitrogen-oxygen) cycle. Nitrogen then undergoes a series of reactions which result in the production of ^{22}Ne. If this isotope of neon exceed the abundance of ^{20}Ne then we usually see the enrinchment of the intershell with ^{27}Al. This is not an He-burning products but is being created during the H-burning shell (Kobayashi et al. (2006), Matteucci (2021) and Karakas & Lattanzio (2014). At the same time, as it has been shown in Karakas & Lattanzio (2014), the metallicity of the AGB star also high influences the yield of Aluminium and it appears to be lower for lower metallictiy stars and vice versa. That being said, SNIa can also produce Al but because in that type of supernova iron is produced in bigger amounts, [Al/Fe] is overshadowed by [Fe/H] and is not as useful to trace SNIa environments. Consequently, stars in the disk and accreted ones can have low [Al/Fe] but they show a difference in the iron-peal, α elements and metallicity.

A very important iron-peak element which also is used as a tracer of SNIa supernovae is Maganese (Mn). Mn shows an increasing trend with metallicity and thus signifies metal rich environments, with a developed stellar population (Feuillet et al. (2022), Das et al. (2020)).

The Milky Way has a fast star formation rate and composes a massive stellar popula-

tion which means that it can sustain and hold the expelled matter from the supernovae. Knowing this, as stellar populations evolve the α to iron abundance is decreasing as iron abundance is increasing. The slope of [α/Fe]-[Fe/H] is steep for Milky Way stars but shallower for stars that are produced in slower formation rates, smaller stellar populations, such as accreted stars (Nandakumar et al. (2024)). The chemical plane described by [Mg/Mn] vs [Al/Fe] functions as a diagnostic tool in order to distinguish in situ and accreted stars. [Al/Fe] depends on the mass and metallicity, thus low [Al/Fe] abundances are expected for both cases, but especially in accreted stars. The α abundances difference is more visible from the [Mg/Mn] relationship than the [Mg/Fe]. As mentioned, Mn is a strong remnant of SNIa and can distinguish better the low-α populations (Das et al. (2020), Feuillet et al. (2022)). Therefore, accreted stars in this chemical field are expected to be located in low [Al/Fe] and high [Mg/Mn]. High [Mg/Mn] in this scale means that the stars were born after enrichment of the ISM with Mn, so a high α environment, and low [Al/Fe] indicates a slower star formation. Since both those value show a delayed stellar evolution compared to Milky Way's, they are assumed to be extragalactic.

The issue, however, with metal rich stars is that the Manganese abundances can highly vary. That is due to the different events that were explained in section 2.4 and thus the NLTE effects can cause a difference of around 0.5 dex in the Mn trend and additionally in the diagnostics graph.

Even though there has been a lot of research in this area and whether the diagnostics graph on its own is enough to determine and pick out extra-galactic stars, there hasn't been research showing whether the NLTE effects change this interpretation or not. And if it does, in what way and whether the same diagnostics graph is of any use or not. Therefore, this thesis project will try to answer those questions and explore how the in-situ and accreted stars behave in this chemical space with abundances determined using models assuming LTE and NLTE.

Chapter 3

Method

3.1 SME and MARCS

The program used to determine the abundances is called SME (Spectroscopy Made Easy). SME creates the synthetic spectrum by solving the radiative transfer equation (Smith et al. (2012)). In order to correctly synthesize the spectrum, the atmosphere of the star must be modeled. The atmosphere model used by SME is called MARCS (Model Atmospheres with a Radiative and Convective Scheme). The assumptions the MARCS model makes to achieve that as described in Smith et al. (2012) is:

- Stratification and hydrostatic equilibrium: this means that the star's atmosphere remains constant. The outwards pressure gradient is counteracted by the star's own gravity which is a force pulling inwards due to the size and mass of a star. This keeps the star in balance.

- Mixing length convection: this theory describes how convection works in the star's outer atmospheric layers. Convection is when due to a high temperature gradient, warm gas rises up and then condenses back to cooler gas and sinks down to the atmosphere. In a star this kind of circulation occurs and the 'mixing length' describes the distance the gas travels before it exchanges energy with the surroundings. So, in a sense it describes the efficiency of the convection happening in the atmosphere of a star in a more simplified way that is still a reasonable energy transport model.

- LTE: The LTE model has been described in 2.4. In short, it assumes a collisional dominated environment where radiation from the star or from other stars does not impact the energy change in the system of the star and the source function equals the Plank function.

- Spherical geometry: This is more important in the way the radiative transfer equation is expressed, where intensity is specified in the direction of the observer. Therefore, depending on the angle of the observer, effects that are affected by the depth at

which our line of sight penetrates the star's atmosphere, such as limb darkening, can be taken into account.

3.2 Sample

In this project, the spectra I will be using and analysing originate from the sky survey APOGEE and of its latest data release, DR17. Furthermore, the sample of around 2000 stars is taken from a sample of 6000 calibrated Kepler stars with accurate log(g) value and specified line and continuous masks. This sample is going to be referred to in this work as the APOKASC (Asteroseismic and Spectroscopic Oscillations of Stars in the Kepler Field) sample. For those stars, estimations for the log(g) value were made via astroseismology as explained in Pinsonneault et al. (2018). As discussed in section 2.3, this method results to more accurate log(g) values and provides better synthetic spectra. Furthermore, uncertainties and errors in this thesis are assumed to be similar to the ones in Fridén (2023). The random uncertainties were calculated using Monte Carlo method since there can be many systematic errors that one cannot estimate accurately, and show the sensitivity of each abundance based on the different stellar parameters (log(g), metallicity, effective temperature). The calculations include three stars that are judged to represent the sample well. Those stars have relatively similar temperatures and log(g) values but differ in metallicity and signal to noise ratio (SNR described in section 3.3). The purpose of the following table is to show that the uncertainties derived in Fridén (2023) should be similar to mine.

Table 3.1: This table shows the three random stars chosen in Fridén (2023) along with their stellar parameters, SNR, T_{eff}, log(g), [Fe/H], v_{mic} (v_{mic} is the microturbulence which is described in section 2.3). Below that the random errors generated for them for the abundances of Aluminum, Magnesium and Manganese are shown.

	2M19375823+4040256	2M19451793+4846592	2M19235187+4529083
SNR	650	670	250
T_{eff} [K]	4350	4700	4750
log(g)	2.38	2.62	2.42
[Fe/H]	0.32	-0.49	-0.08
v_{mic}	1.09	1.21	1.27
σ[Al/Fe]	0.12	0.11	0.11
σ[Mg/Fe]	0.08	0.08	0.08
σ[Mn/Fe]	0.08	0.10	0.10
σ[Fe/H]	0.06	0.06	0.06

According to the values in table 3.1, for [Al/Fe] the error is 0.113, for [Mg/Fe], 0.080 and for [Mn/Fe], 0.093. For the diagnostic plot that has y-axis [Mg/Mn], the difference of [Mg/Fe] and [Mn/Fe] is taken so the error is estimated to be $\sigma[\text{Mg/Mn}] = \sqrt{\sigma[\text{Mg/Fe}]^2 + \sigma[\text{Mn/Fe}]^2} =$

0.123.

Moreover, in Fridén (2023), there is an important comparison between the newly derived abundances by SME and the ones that were derived by APOGEE using the pipeline ASPCAP, "APOGEE Stellar Parameters and Chemical Abundances Pipeline". ASPCAP extracts abundances by firstly fitting the whole obtain spectrum to determine the stellar atmospheric parameters such as temperature and log(g) and then chose a specific range showing strong spectral features for a chosen element and determines the abundance (Pérez et al. (2016)). However, this method cannot be fully trusted because perhaps the whole spectrum is not reliable and contains bad pixels which then result to not accurately estimated parameters. Even though APOGEE includes flags with warnings about bad stars that the spectrum may be affected by neighbors being to bright or just a bad signal to noise ratio, a more detailed approach is needed. Therefore, using stars from Fridén (2023), a better log(g) was used and good spectral lines as well as continuum masks which were chosen manually to avoid bad pixels and unreliable lines were also used.

In figure 3.1 I show an example of a synthesized spectrum using SME which determined the abundance of Aluminum to Iron in NLTE for a random star in the ≈ 2000 stars sample.

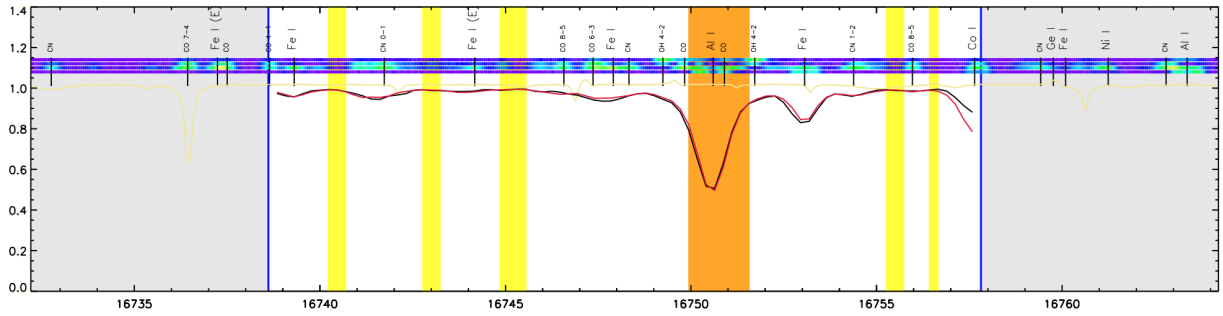

Figure 3.1: In black is fitted with the spectrum synthesized by SME in red. The yellow masks are the continuum masks that the average slope of the observed spectrum is almost zero. The orange masks are the lines masks which are specific for each element. The light yellow spectrum is the absorption spectrum due to the Earth's atmosphere which must be taken into account also when synthesizing the spectrum. Lastly, the colorful/rainbow bar on the top shows how sensitive the different molecular/atomic lines (also shown in the bar) are with respect to the surface gravity, effective temperature, metallicity and micro- and macroturbulence

Moreover, it is important to note that for each spectrum, the vmac was initially calculated and then used as a set parameter to determine abundances. The reason APOGEE's vmac was not utilized is because it was estimated through their own derived metallicities via ASPCAP using the formula $vmac = 10^{0.4710.254[\mathrm{M/H}]\ 1}$. In this case, using SME, one can set the parameter of vmac and radial velocity as free parameters and estimate vmac as it synthesizes the spectrum and fitting the six chosen Fe I lines mentioned in Fridén

[1] [M/H] stands for the the abundance of elements heavier than helium in a star

(2023). Lastly, in Fridén (2023), many data points were excluded due to very low and even negative vmac:s being estimated, so in this project, in order to avoid losing a lot of valuable data, I increased the resolution used for the χ^2 (see point 6 chapter 3.3) to 20000 from 15000 which then resulted to bigger and non negative vmac values (around 12). In this way, vmac includes corrections for the resolution and instrumental profile of the spectrum.

3.3 Conditions for accreted stars

As mentioned before, the "metric" that I employ to determine whether abundances can be used solely for determining accreted stars, is a sample of 88 stars of extragalactic origin chosen out of a greater sample of 675,000 stars in APOGEE survey. In order to pick those out, the conditions suggested in Feuillet et al. (2022) were used and are:

1. $SNREV > 80$: Describes the Signal-to-Noise Ratio per Resolution Element in the near-infrared (NIR) spectra (SNREV). A high number indicates a high resolution signal that is greater than the background noise. In this case we are only allowing signal that are 80 times higher than the background noise (SDSS-IV Collaboration (2021)).

2. AL_FE_FLAG = 0: The flag shows whether the aluminum to iron abundance is reliable or not and since APOGEE is using bit code, 0 means it is and 1 means it is not, so we are taking into account stars for which that the aluminum abundance is reliable (SDSS-IV Collaboration (2021)).

3. $4000K < TEFF < 6000K$: Sets the limits for the effective temperature, as shown for stars between 6000K and 4000K, taking into account F, K and G-type stars.

4. $LOGG < 2.8$: The surface gravity of the stars is less than 2.8. The reason for that is that lower log(g) targets are bigger and cooler giant stars which then (as discussed in section 2.3) are the types of stars whose spectra contain spectra lines that are less contaminated and more reliable to be used for abundance analysis. In this sample, log(g) is also calibrated with the log(g)-value derived for Kepler stars using astroseismology.

5. Remove any VERY_BRIGHT_NEIGHBOR and PERSIST_HIGH bit set in STARFLAG: A set of flags associated with spectral processing, radial velocity, and spectral combination. The ones chosen to be omitted were stars that had a neighbor object 100 times brighter than them and more than 20% of the pixels in the spectrum were in high persistence region (SDSS-IV Collaboration (2021)).

6. Remove any STAR_BAD, CHI2_BAD, M_H_BAD, and CHI2_WARN bit set in ASPCAPFLAG: Set of flags that are associated with errors in the ASPCAP fits. The stars excluded were those that showed any error results for log(g), T_{eff}, color, S/N ratio, χ^2 or rotation for the "$STAR\_BAD$". For "$CHI2\_BAD$" and "$CHI2\_WARN$"

stars that had $\chi^2 > 50*(SNR/100)**2$ where left out. In statistics, χ^2 expresses the discrepancy of the best fit model of the recorded data and the actual raw data. In the context of a stellar spectrum, χ^2 shows the discrepancy between the observed and synthetic spectrum made using the determined stellar parameters. Lastly, "M_H_BAD" indicates whether a measurement of a metal abundance (not hydrogen or helium) is not trustworthy (SDSS-IV Collaboration (2021)).

7. Remove duplicate observations of a single target that have bit 4 of the EXTRATARG set: Removes duplicate observations of the same star.

8. $\sigma_\pi/\pi < 0.2$: Considers the parallax of the observation to choose stars with reliable distances.

9. $V_{rot} < 110km/s$: In Feuillet et al. (2022), they argue that Halo velocities are $< 110km/s$, so with this condition they want to find halo like rotational velocities in disk stars which is an indicator that the star is moving in opposite direction and thus might be of extragalactic origin.

10. $[Al/Fe] < -0.2$: Chooses aluminum abundance less than -0.2 due to the low aluminum metallicities criterion for accreted stars (see section 2.5).

Hence, with reference to the theory covered by sections 2.3 and 2.5, the conditions aim to select stars that due to both abundances and kinematics should be accreted. The other stellar parameters and flags used are just to make sure the sample has reliable spectra. Yet, even though abundances are calculated for those stars through the ASPCAP pipeline, as explained in Fridén (2023), the method APOGEE uses can result to not as precise values and a more careful manual approach is advised. I will be using the same lines lists as in the APOKASC sample. After getting the values of [Al/Fe], [Mg/Fe] and [Mn/Fe] both in NLTE and LTE, using SME I will finally construct the diagnostic graph of [Mg/Mn] vs [Al/Fe] and see where those 88 stars fall. Moreover, for those 88 stars, each spectrum was also carefully investigated in this thesis and slightly altered line and continuum masks were chosen in order to avoid bad synthetic fitting.

Chapter 4

Results and Discussion

In this chapter, the determined abundances both for LTE and NLTE will be shown for the elements Mg, Mn and Al for for the 2000 APOKASC Milky Way field stars and 88 extragalactic stars chosen from Feuillet et al. (2022). Then, using those values the diagnostics graph is constructed and analyzed. Finally, I will discuss the results and possible conclusions.

4.1 Abundances

The abundance for the elements Al, Mg and Mn is derived for 1944 APOKASC stars instead of 2000 due to some bad spectra which had to be omitted.

Starting with Mn, the graph in figure 4.1a shows the determined values. In black dots is the NLTE derived values and in grey dots the LTE ones for the APOKASC sample. As one can see from this graph, there is a clear discrepancy between the trends. Even thought the trend is the same, the NLTE values are sitting a bit higher. As described in section 2.4, the NLTE corrections increase with metallicity for iron-peak atoms such as Mn, which then can justify this shift. A greater shift shows a greater correction and in that way we can see the importance of also implementing NLTE corrections in abundances. To show this difference, a graph with axis $Mn_{NLTE} - Mn_{LTE}$ is constructed as shown in figure 4.1b. A color-bar which is color coded with the effective temperature of each star is used in order to check if there could be any other reasons for such a shift and also see the effect of temperature in such abundance determinations. From figure 4.1b, the absolute difference between the LTE and NLTE values is around 0.15 dex and has a rising trend with the stars showing low scattering. The color-bar allows us to see that we have lower differences for cooler stars and higher differences for warmer stars. This demonstrates the effect of temperature in the NLTE corrections. As explained in Chapter 2.2, higher temperatures imply more collisions resulting in the broadening of the spectra lines. Yet, in this case even the warmer stars do not exceed 5500K which categorizes them into G-type stars which are considered cool stars. So, from this graph we can conclude that temperature is not a factor

for this variation.

The accreted stars sample are following the same pattern, with NLTE located higher than LTE. The only bigger difference is in the variation of temperature in figure 4.1b. In that plot the stars follow the upwards trend and are positioned at the end of the tail with cooler stars on the bottom and warmer on the top at higher NLTE corrections. The range of temperatures is higher, reaching around 5200 for some of them. Moreover, it is interesting to see that accreted stars do overlap with the APOKASC sample but sort of follow the trend going downwards.

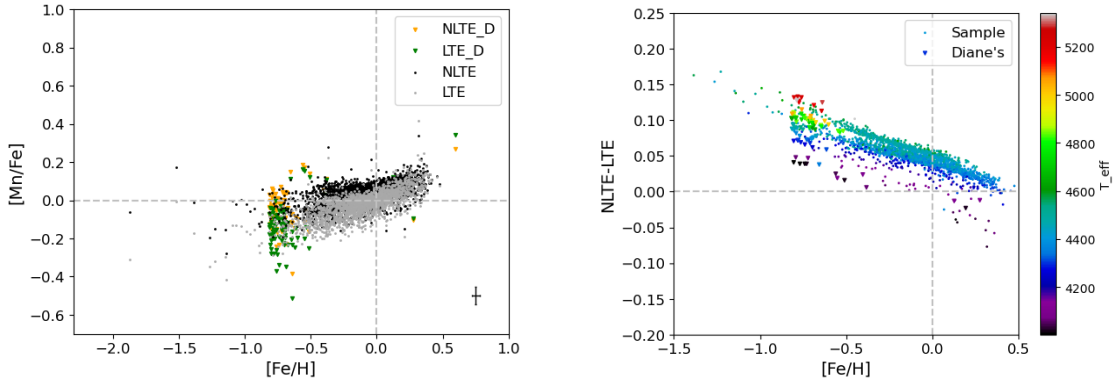

(a) (b)

Figure 4.1: The figure in left shows the calculated abundances for Mn. On the x-axis is the iron abundance [Fe/H] and on the y-axis the Manganese abundance, [Mn/Fe]. Black and grey dots represent abundances with NLTE and LTE respectively. The orange inverted triangles represent the 88 accreted stars for which abundances were determined using NLTE and green inverted triangles denote the LTE abundances. For the figure on the right, the absolute value between the difference of the NLTE and LTE value was taken and plotted on the y-axis, whilst on the x-axis the iron abundances [Fe/H] are plotted. The iron abundance did not change for LTE or NLTE because the same mactoturbulence values were derived for both cases from the same Fe I lines. The uncertainty is 0.06 for [Fe/H] and 0.09 for [Mn/Fe].

The figure 4.2a is assembled with the aluminium abundances determined in the same way. For this element, the opposite is observed. The NLTE values sit lower than the LTE ones. Since Al is also in the category of photoionization atoms (see section 2.4), a decrease in NLTE corrections should imply higher metallicity. In this case we can see that the absolute difference is of around 0.60 dex which is a lot and again the temperature variation is the same as for Mn (figure 4.2b). Regarding the accreted sample shown with orange and green for NLTE and LTE respectively, the values are lower than the APOKASC sample which is reassuring and follows the theory explained in 2.5. Accreted stars theoretically should have lower [Al/Fe] and this is successfully shown here. Besides, the temperature range is similar to that of Mn, but the corrections are smaller and very similar for all the

88 stars. That is probably due to the restricting factor or $[Al/Fe] < -0.2$ implying there are less corrections for lower aluminum abundances.

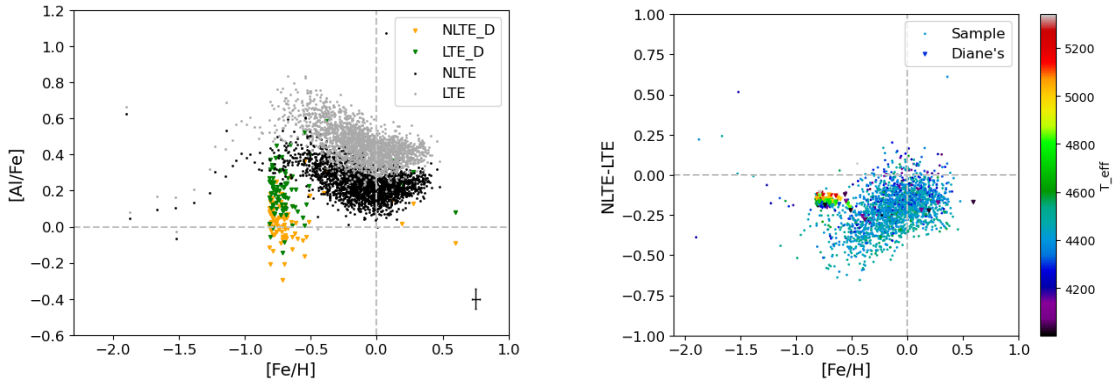

(a) (b)

Figure 4.2: In the left figure, black and grey points represent the abundances for Aluminum for NLTE and LTE respectively for the APOKASC sample. In the same way, green inverted triangles show the NLTE and orange inverted triangles the LTE derived abundances for the accreted sample. In the right figure, the absolute difference between NLTE and LTE is shown.The uncertainty is 0.06 for [Fe/H] and 0.11 for [Al/Fe].

Unlike figure 4.1a, the Aluminum abundances shown in 4.2a do not pass through the solar value (0,0) and they appear very much higher. That is probably an issue with the solar normalization scale. This can be problematic because condition number 8 in section 3.3 specifically selected stars with $[Al/Fe] < 0.2$ in LTE. However, in this graph (4.2a), the green inverted triangles that denote those stars are located very much higher, close to -0.1. In order then to make sure that the data can still be used, I normalized the APOKASC sample with the APOGEE one. According to APOGEE, Al abundances were obtained using LTE so I moved the APOKASC sample determined with LTE by -0.23 which was the amount needed to have an overlap between my LTE determinations and the values provided in the APOGEE DR17 catalog for the APOKASC sample (see Appendix 1). In that case, shifting the accreted stars also by the same amount should result in the correct abundances and finally, even though the data do not pass through the solar values, are still reliable to be used and draw conclusions from.

Lastly, the plots for Mg are shown in figure 4.3a,b. Here a similar shift as for Al is observed. The NLTE values sit lower than the LTE and the color coded graph (figure 4.3b) is similar to Mn in a sense that there is less scattering and a clear descending trend. Yet, the temperatures here do not vary a lot and do not follow the pattern like in the other two cases, so no conclusions can be drawn from that.

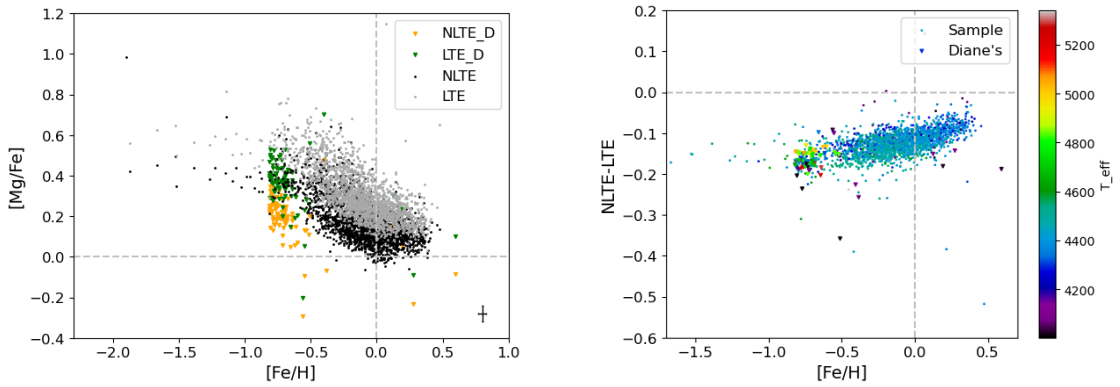

(a) (b)

Figure 4.3: The same construction of those plots as for figures 4.2a,b and 4.1a,b is shown with y-axis [Mg/Fe] and x-axis [Fe/H]. The uncertainty is 0.06 for [Fe/H] and 0.08 for [Mg/Fe].

4.2 [Mg/Mn]-[Al/Fe]

Having now collected all the data for both the APOKASC and accreted stars sample, the diagnostics graphs can be made. In order to do so, as described in section 2.5, on the y-axis we need to have [Mg/Mn] and in the y-axis [Al/Fe]. So, knowing that bracket notation for abundances refers to logarithmic values (see chapter 2.3), the x-axis is set up by subtracting the [Mn/Fe] from [Mg/Fe], like the following:

$$[\mathrm{Mg/Mn}] = [\mathrm{Mg/Fe}] - [\mathrm{Mn/Fe}] \tag{4.1}$$

The final plot is shown in figure 4.4, with the same color scheme for the accreted and the APOKASC sample.

The plots in figure 4.4 in the bottom are the most important for this project. As discussed in chapter 2.5, accreted stars are positioned in low [Al/Fe] values and high [Mg/Mn] values. However, previous works mentioned in chapter 2.5 have explored this chemical space with abundances determined in LTE. Looking at the LTE trend in the bottom left plot, it looks very similar to other ones seen in Das et al. (2020), Feuillet et al. (2022) and Ceccarelli et al. (2024), with the acrreted stars (green points) located on the side of the trend of the disk stars. However, if we have a look at the NLTE values, we see that the trend changes a lot, yet a similar pattern is still conserved. The black dots that show the NLTE values for the APOKASC sample, stand up straight at relatively non-changing Al metallicities, but show an increase in the [Mg/Mn] axis which mathematically, using equation 4.1, it implies a lower (or negative) Mn abundance. On the other hand, the orange stars are positioned in low [Al/Fe] as expected but not as high [Mg/Mn]. Still, accreted sample is on the higher [Mg/Mn] values relative to the black ones and also do not exactly overlap with the sample but are next to it on the left, like for the LTE case. So, as a result, the overall trend is there but NLTE corrections show that the APOKASC values become

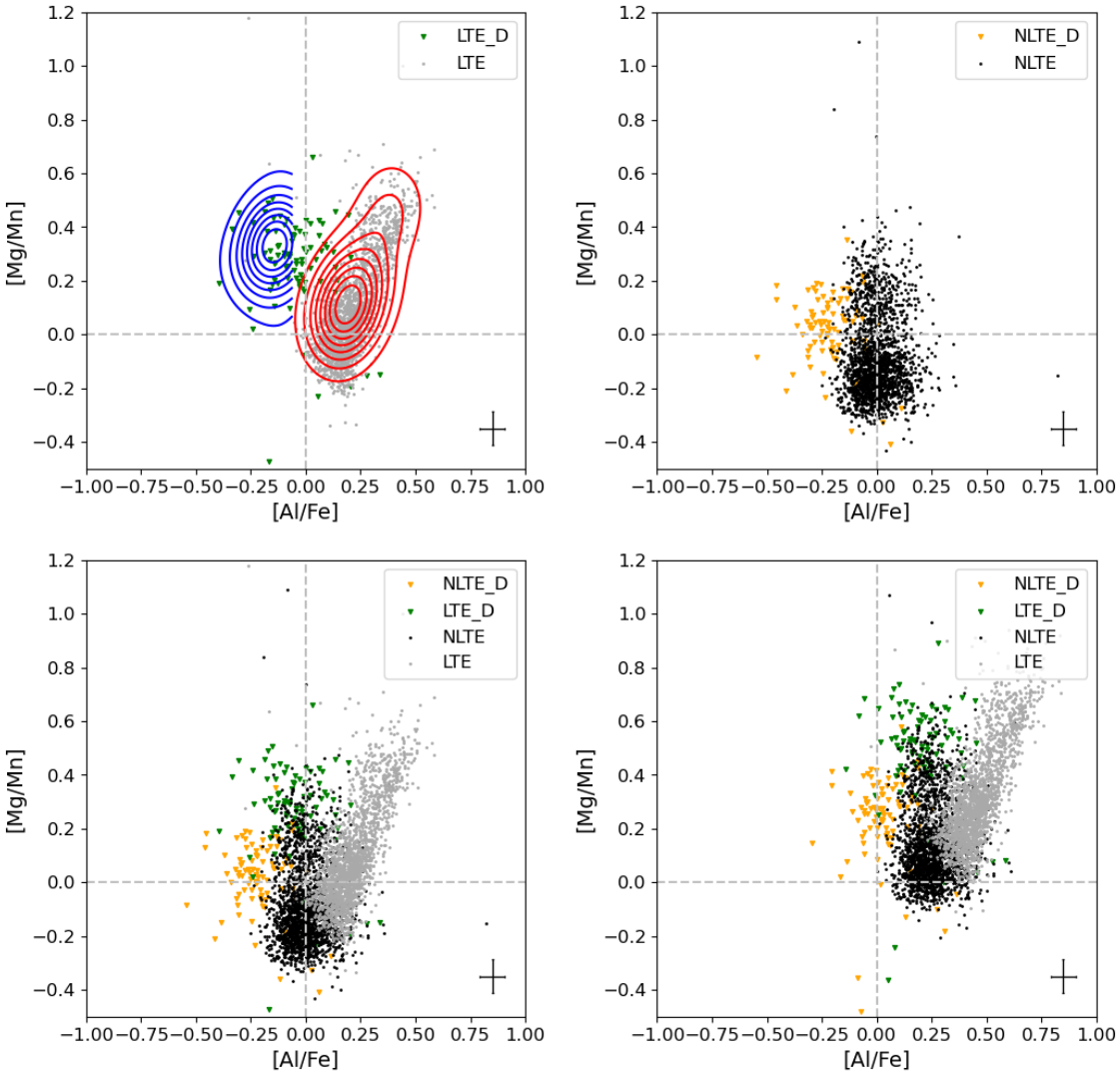

Figure 4.4: On the top left corner are only the LTE values for the accreted (green inverted triangles) and the APOKASC sample (grey points). The contour lines show the population of the APOGEE values and is used as a benchmark to show that their LTE and my LTE determinations are overlapping. On the top right corner, the NLTE values are shown for the accreted stars (orange inverted triangles) and the APOKASC sample (black points). Both top graphs and bottom left are shifted uniformly by the same amount my LTE values needed to be shifted to match APOGEE's (see Appendix 1). The color scheme is the same for the bottom left graph as for the abundance graphs. Lastly, on the bottom right corner is the same graph as the bottom left, but purely using the derived values, without any shifting. The uncertainty is 0.12 for [Mg/Mn] and 0.11 for [Al/Fe].

even closer than with LTE. In order to demonstrate this better, I created a contour for the LTE and NLTE, for the APOKASC and accreted sample, using Gaussian statistic in

python to show the difference in the population of each sample. Figures 4.5a and 4.5b show how much closer and overlapping the contour lines are for the NLTE case than the LTE case, with a greater union area of the two contours.

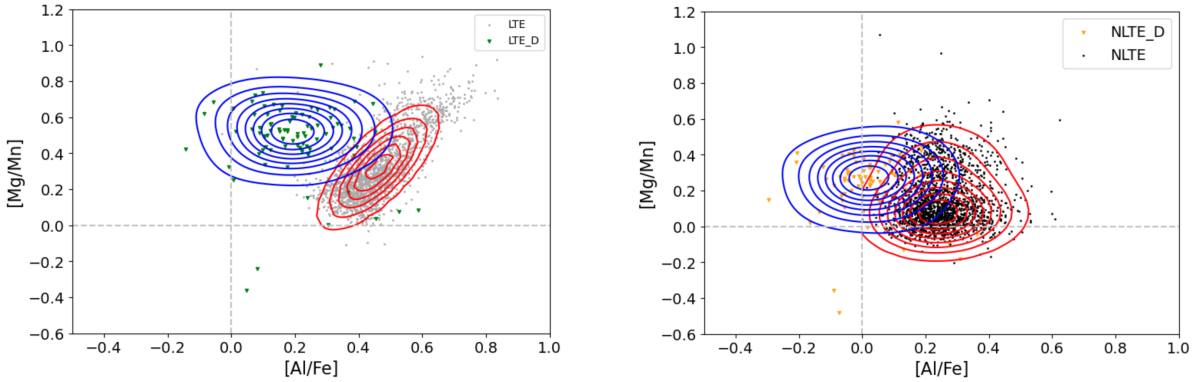

(a) (b)

Figure 4.5: The red contour lines show the population of the APOKASC sample for LTE and NLTE represented by grey and black points respectively in the left and right plot. Same follows for the accreted star sample contoured with blue lines and represented by green and orange inverted triangles for LTE and NLTE respectively for the left and right side plot.Axis for both plots are [Mg/Mn] for y-axis and [Al/Fe] for x-axis.

Another reason this big of a change is observed might also be due to the lines used for Mn. Mn undergoes hyperfine splitting with causes broadening effects and influences the line strength. This not taken into account for because no models that can estimate that effect accurately in the log(gf) value have been developed yet. Lastly, the amount of lines used could also be a source of issue. The more lines, the better the estimation of the actual abundance of those elements. More lines allow greater comparison and reduce uncertainties. In this project, for Al, three lines were used, for Mn, two lines were used and for Mg only one line was used. Lastly, uncertainty error as shown in section 3.2 cannot be a possible source for such a change as the error is random, not systematic and relatively very small.

Chapter 5

Conclusions

Looking at the bottom right graph in figure 4.4, there is a indeed a difference between LTE and NLTE and as emphasized in Eitner et al. (2019), indeed a NLTE approach is very crucial especially for abundance of Mn and Mg. Yet, sadly it does not reveal a clear pattern that indicates that those stars are of extraglactic origin. Although not overlapping with the sample, they are very close and had they not been marked as accreted, they maybe would had been assumed to be outliers. Therefore, main conclusion for this project is that such a chemical plane constructed from abundances derived with NLTE cannot be used on its own to distinguish in-situ and accreted stars. Yet, it shows that when implementing NLTE, that method does not help in the search of extragalactic stars. As suggested from various studies (such as Vasini et al. (2023), Das et al. (2020), Feuillet et al. (2022)), other information such as retrograte velocities and stellar ages are some other stellar parameters that could also be handy if used with this diagnostic graph.

Future outlook

For the future outlook, according to the results obtained from this projects, it is advised to use NLTE corrections too because they do show substantial differences with LTE. It will be ideal to have more efficient NLTE grids that will reduce computational time. Even though the NLTE method might appear more realistic, using it is not always optimal. The amount of uncertainties coming along with the different collisional and radiative coefficients calculated can be very high making the end result not reliable enough to utilize. Moreover, the commonly used models are made for an 1D hydrostatic atmosphere which needless to say is far from the 3D object we are observing. Those being the main drawbacks, along with long computing time are the reasons scientists usually use LTE.

Thus far, errors related to atomic data and atmospheric models are highly related to the strength of the lines and they are the most impactful when determining abundances. In the paper Andersson et al. (2015), the researchers developed a theoretical method which tries to tackle the broadening effect due to hyperfine structure using three Mn I lines at

17325, 17339, and 17349 Å. The results showed how much the log(gf) was affected, which as explained in the paper is very crucial when fitting synthetic spectra. Therefore, trying to account for such atomic data discrepancies and developing models accounting for hyperfine structure could be a fruitful approach for a finer estimation of the line strength in the infra red (also shown in Montelius (2021)).

Moreover, another method suggested in the paper Vasini et al. (2023), is to try to find other diagnostic plots, for example using s-process elements. s-process elements are also called slow neutron capture elements. Those are elements that are formed by neuron capture processes and are heavier than iron (Matteucci (2021)). That includes many elements but the most significant for stellar investigations have shown to be Ba, Y and Zr. As seen in Magrini et al. (2018), stars that have more than 70% s-process elements are younger, which is expected since s-process elements take billions of years to be produced in a star and then when the star dies, such elements are expelled in the ISM. Like for Al and Mn, it is said that heavier elements are produced in massive stars so they are expelled through SNII supernova. Yet, this is just to be used as a further aid to a chemical investigation for accreted stars.

Acknowledgements

I would like to thank my supervisors Govind Nandakumar and Nils Ryde for all the support and knowledge I received through this process. Their help was very insightful and I am very happy they chose to work with me. Also, I am very grateful for the weekly meetings both with the ISA team and the supervisors and the constructive feedback I was given.

Bibliography

Andersson, M. et al. 2015, The Astrophysical Journal Supplement Series, 216, 9

Bergemann, M. & Nordlander, T. 2014, NLTE Radiative Transfer in Cool Stars: Theory and Applications to the Abundance Analysis for 24 Chemical Elements (Springer International Publishing), 169–185

Ceccarelli, E., Massari, D., Mucciarelli, A., et al. 2024, Astronomy & Astrophysics

Das, P., Hawkins, K., & Jofré, P. 2020, MNRAS, 493, 5195

Eitner, P. et al. 2019, Astronomy & Astrophysics, 617, A106

Feuillet, D. K., Feltzing, S., Sahlholdt, C., & Bensby, T. 2022, The Astrophysical Journal, 934

Forsberg, R. 2023, PhD thesis, Lund University

Fridén, E. 2023, Master's thesis, Lund University

Gray, D. F. 2022, The observation and analysis of stellar photospheres

Jofré, P., Heiter, U., & Soubiran, C. 2019, ARA&A, 57, 571

Karakas, A. I. & Lattanzio, J. C. 2014, , 31, e030

Kobayashi, C., Umeda, H., Nomoto, K., Tominaga, N., & Ohkubo, T. 2006, ApJ, 653, 1145

Magrini, L. et al. 2018, Astronomy & Astrophysics, 617, A106

Matteucci, F. 2021, , 29, 5

Montelius, M. 2021, Master's thesis, Lund University

Nandakumar, G., Ryde, N., Forsberg, R., et al. 2024, Astronomy & Astrophysics, 684

Pinsonneault, M. H., Elsworth, Y. P., Tayar, J., et al. 2018, The Astrophysical Journal Supplement Series, 239

Pérez, A. E. G., Prieto, C. A., et al. 2016, The Astronomical Journal, 161

Renaud, F., Agertz, O., Read, J. I., et al. 2021, MNRAS, 503, 5846

Rocco, H. O. D. & Cruzado, A. 2012, Acta Physica Polonica A, 122, 666

Rutten, R. J. 2003, Radiative Transfer in Stellar Atmospheres, 8th edn. (Utrecht University), lecture notes

SDSS-IV Collaboration. 2021, APOGEE Bitmasks Documentation, SDSS-IV

Smith, V. A., C., J. H., & Holtzman, J. A. 2012, SME: Spectroscopy Made Easy: User Manual, STScI

Vasini, A., Spitoni, E., & Matteucci, F. 2023, Astronomy & Astrophysics

Appendix A

Normalization graphs

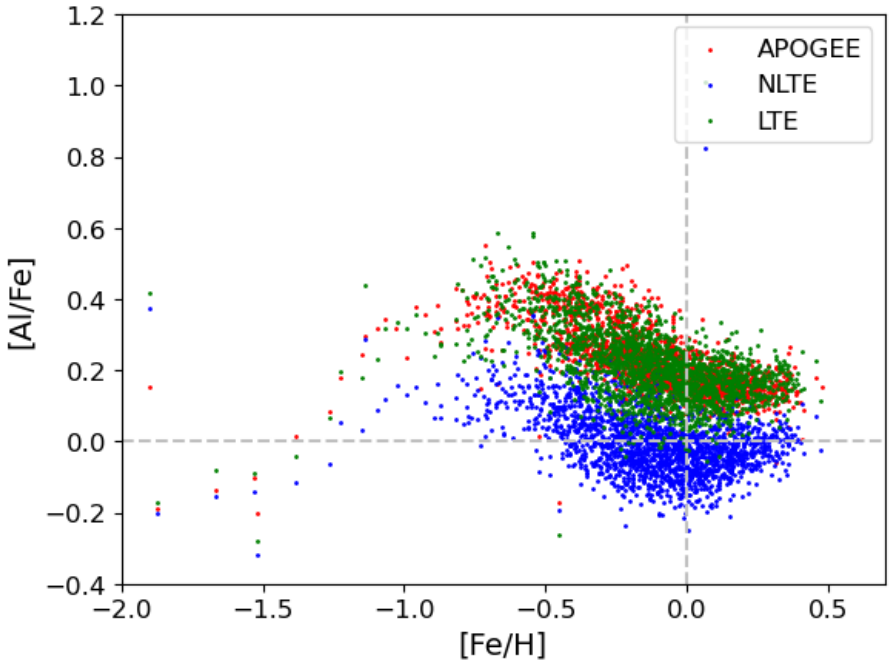

Figure A.1: This plot shows how the abundance values of Al in NLTE and LTE can be normalized by being shifted. Red marks denote APOGEE's values, green, LTE and blue, NLTE. The shift aims to match the LTE values with APOGEE's values since they have determined the LTE abundances and normalized them with the solar values. The shift needed to be -0.25 in the y-axis to make this match. This figure is to be used as a benchmark

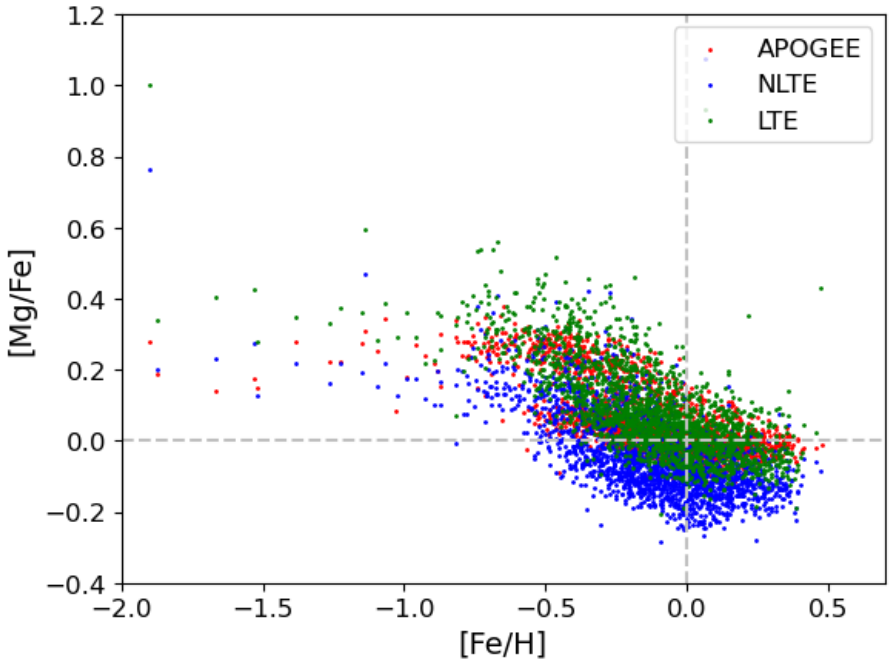

Figure A.2: This plot shows how the abundance values of Mg in NLTE and LTE can be normalized by being shifted. Red marks denote APOGEE's values, green, LTE and blue, NLTE. The shift aims to match the LTE values with APOGEE's values since they have determined the LTE abundances and normalized them with the solar values. The shift needed to be -0.23 in the y-axis to make this match. This figure is to be used as a benchmark

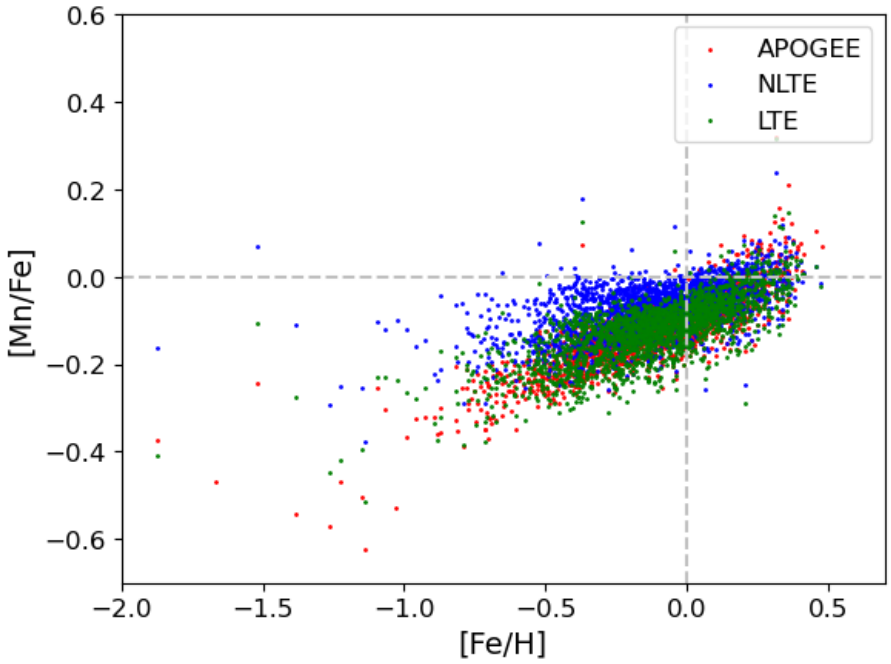

Figure A.3: This plot shows how the abundance values of Mn in NLTE and LTE can be normalized by being shifted. Red marks denote APOGEE's values, green, LTE and blue, NLTE. The shift aims to match the LTE values with APOGEE's values since they have determined the LTE abundances and normalized them with the solar values. The shift needed to be -0.10 in the y-axis to make this match. This figure is to be used as a benchmark